

Oil & Natural Gas Technology

DOE Award No.: DE-FE0010406

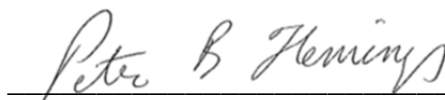
DUNS No. : 170230239

Quarterly Research Performance Progress Report (Period ending 3/31/2013)

CONTROLS ON METHANE EXPULSION DURING MELTING OF NATURAL GAS HYDRATE SYSTEMS: TOPIC AREA 2

Project Period (1/1/2013 to 3/31/2013)

Submitted by:
Peter B. Flemings



Signature

The University of Texas at Austin
101 East 27th Street, Suite 4.300
Austin, TX 78712-1500

e-mail: pflemings@jsq.utexas.edu

Phone number: 512-475-9520

Prepared for:
United States Department of Energy
National Energy Technology Laboratory

April 30, 2013



Office of Fossil Energy



ACCOMPLISHMENTS:***What are the major goals of the project?***

The project goal is to predict, given characteristic climate-induced temperature change scenarios, the conditions under which gas will be expelled from existing accumulations of gas hydrate into the shallow ocean or directly to the atmosphere. When those conditions are met, the fraction of the gas accumulation that escapes and the rate of escape shall be quantified. The predictions shall be applicable in Arctic regions and in gas hydrate systems at the up dip limit of the stability zone on continental margins. The behavior shall be explored in response to two warming scenarios: longer term change due to sea level rise (e.g. 20 thousand years) and shorter term due to atmospheric warming by anthropogenic forcing (decadal time scale).

Milestone Description	Planned Completion	Actual Completion	Verification Method	Comments (progress toward achieving milestone, explanation of deviation from plan, etc.)
1.A 1-D simulation of gas hydrate dissociation in natural systems.	9/30/2013		Report	We plan to continue using the Buckley-Leverett equations to set the parameters for our experimental goals. We hope to fully capture the gas saturation profile during the gas flooding stage of the experiment using this approach.
1.B 1-D Simulation of gas hydrate dissociation in laboratory controlled conditions.	3/31/2014		Report	Developed thermistor string for use in experimental device; , did preliminary simulations of gas flooding.
1.C Model-based determination of conditions required for gas not to reach seafloor/atmosphere from dissociating hydrate accumulation.	3/31/2014		Quarterly Report	
1.D Determination of what hydrate reservoirs are at three-phase equilibrium.	12/30/2013		Report	Evaluating petrophysical basis for large saturation exponents for resistivity in sediments with large hydrate saturation. Applying approach to known reservoirs. Significant progress on this. See comments below
1.E Demonstrate ability to create and dissociate methane hydrate within sediment columns under conditions analogous to natural systems.	9/30/2013		Report	Currently developing/refining remote-sensing technologies for experimental apparatus. Thermister string developed.
2.A 1-D simulation of gas expulsion into hydrate stability zone.	9/29/2014		Report	Preliminary simulations produced
2.B Determination of conditions for which gas expulsion into hydrate-stability zone is self-limiting.	12/29/2014		Report	
2.C Demonstration of reaction	9/30/2014		Quarterly	Currently developing/refining

transport experiment where gas invades hydrate stability zone and creates three phase stability.			Report	remote sensing technologies.
2.D Demonstrate a 2D simulation of hydrate dissociation and gas expulsion.	3/31/2015		Report	

What was accomplished under these goals?

Task 1: Project Management and Planning:

In the last quarter, we hired one post-doctoral scientist and recruited one student graduate student. The student is now working full time on the project and will start classes in the fall of 2013. The post-doctoral scientist, NAME, will arrive from Texas A&M on June 15, 2013. We have continued to have bi-monthly meetings with LBNL and between the Department of Geological Sciences and the Dept. of GeoSystems and Petroleum Engineering.

Task 2: Conceptual and Numerical Model Development -1D:

Subtask 2.1 - Dissociation of 1D vertical hydrate accumulation

Subtask 2.2 - Apply 1D model to laboratory experiment

Subtask 2.3 - 1D models of natural examples

Subtask 2.3.1 Hydrate accumulations below permafrost

Subtask 2.3.2 - 1D model application to deposits near up-dip limit of stability zone on continental margins

We have begun developing and applying a one dimensional model of hydrate solidification coupling heat and salinity. Initial results simulate gas flux toward the seafloor and solidification due to cooling near the seafloor.

Task 3: Categorize stability of known hydrate reservoirs:

The Recipient shall review and categorize the stability state of existing well-studied hydrate reservoirs, including but not limited to the Cascadia margin at Sites 1249 and 1250 (ODP Leg 204) and U1328 (IODP Exp. 311), offshore India (e.g. the Krishna-Godavari (K-G) Basin and the Ulleung Basin), and the Mallik, and Mt. Elbert deposits, to determine and catalogue their thermodynamic state, i.e. their location relative to the three-phase equilibrium surface. Specifically, the Recipient shall study well-documented examples where pore fluid salinity, temperature, and hydrate saturation are independently measured (e.g. by pore water sampling, and geophysical logs, respectively). The Recipient shall calculate the in-situ pore fluid salinity and shall calculate whether, given the observed temperature, pressure and salinity, the reservoir is at the three phase equilibrium or within the brine-hydrate region (L+H). The Recipient shall develop a public and broad database of well understood examples where the thermodynamic state can be described.

A) Determining in situ gas hydrate saturation, salinity, and thermodynamic state of natural, hydrate-bearing sediments

i. Introduction

We present a method to determine the in situ water saturation and salinity using log and core-derived data. Many studies have focused on the use of resistivity logs in determining the water saturation in hydrate-bearing sediments (Pearson, et al., 1983; Cook, et al., 2010; Cook, et al., 2012; Collett, et al., 2012; Liu and Flemings, 2006). The accuracy of these measurements is still in question,

however, due to unknowns concerning the formation of hydrate in the sediment. The three main issues expressed with this method are:

Limitations of Archie's Law: The primary relationship used in this method was developed by Archie (1941) and was modeled after clean, water-saturated sandstones. This method provides a first-order understanding of the relationship between resistivity and porosity and water saturation. Natural systems, however, frequently have clay content, which affects both the porosity and the resistivity of the formation. This fact has made the accuracy of Archie's Law in natural sediments a consistent point of discussion.

Hydrate Formation: In clean, highly porous sandstones, hydrate is assumed to be fairly evenly distributed throughout the pore space. In nature, however, systems consist of fine, inter-bedded layers of higher and lower permeability sediments. Arguments have been made that hydrate will preferentially form in the layers with high permeability (Daigle and Dugan, 2011). Since the thickness of these layers can be finer than the resolution of the resistivity tools, the measured resistivity may not accurately represent the resistivity of each layer.

Resistivity Anisotropy: There are concerns that the relative angle between the drill string and bedding planes or hydrate-filled fractures may cause significant changes in the measured resistivity (Cook, et al., 2010). One study showed that resistivity measurements parallel to the bedding planes were significantly lower than those perpendicular to the bedding, both in theoretical and natural examples (Cook, et al., 2012). Another study compared hydrate saturations calculated through Archie's Law to those determined through degassed pressure cores and found that the pressure cores had significantly lower hydrate saturations than the Archie-calculated values. The explanation for this was that the presence of fine, near-vertical, hydrate-filled fractures greatly increased the resistivity of the formation with minimal hydrate saturation by forcing the current to take a highly tortuous path (Cook, et al., 2010).

Despite the limitations of Archie's Law presented here, the use of resistivity logs to determine water saturation in unclean sands has been used in industry and research for decades. Therefore, we see it as a good starting point for this portion of the project.

ii. Methods

The study sites were chosen because the presence of hydrate had been previously confirmed and the necessary Logging-While-Drilling (LWD) and core data were available. For each of the wells tested, the first step is to collect the necessary LWD and core-derived data from the time the well was drilled.

An iterative implementation of Archie's Law is used to determine water saturation. This relationship is dependent on resistivity, porosity, and several coefficients and exponents:

$$S_w = \sqrt[N]{\frac{a \cdot \rho_w}{n^m \cdot \rho_t}}$$

Where S_w is the fractional water saturation, N is the saturation exponent (dimensionless), a is the tortuosity coefficient (dimensionless), ρ_w is the fluid resistivity (m), n is the fraction porosity, m is the cementation exponent (dimensionless), and ρ_t is the formation resistivity (m). The fluid resistivity is determined using Arps' Equation (Arps, 1953):

$$\rho_w = 0.0123 + \left(\left(\frac{3647.5}{C^{0.955}} \right) \cdot \frac{45.4}{(T_f + 21.5)} \right)$$

Where C is the fluid salinity (ppm) and T_f is the fluid temperature ($^{\circ}\text{C}$). We use the geothermal gradient to determine the fluid temperature at depth and, initially, use linear interpolation between core-derived chloride concentrations to determine the salinity. Salinity is converted to ppm, by assuming that seawater consists of exclusively chloride and sodium ions at a ratio of 1:0.86.

The cementation and tortuosity coefficients are usually assumed to equal 2 and 1, respectively. For hydrate-bearing sediments, however, these coefficients have been shown to vary enough that they must be determined separately for each site (Spangenberg, 2001). To accomplish this, first the log-derived bulk density data is converted to porosity through the following equation:

$$n = (\rho_m - \rho_b) / (\rho_m - \rho_w)$$

Where n is the fractional porosity, ρ_m is the grain density (g/cm^3), ρ_w is the fluid density (g/cm^3), and ρ_b is the bulk density (g/cm^3). The resistivity and porosity are first filtered to account for resolution differences in the tools. We select data to determine the saturation exponent in the following manner.

- We use data from beneath the Bottom simulating Reflector (BSR) to assure that no hydrate is present in the pore space.
- We use data where the logging while drilling (LWD) data and core-derived bulk density data do not significantly vary in order to eliminate zones where free gas may be present.
- We used data where the bulk density correction does not exceed $\pm 0.25 \text{ g}/\text{cm}^3$ and the caliper does not exceed 2 inches more than the bit diameter to assure that borehole conditions were acceptable during logging operations.

These filters are applied not only to remove points where borehole conditions may have compromised the log data accuracy, but also to assure that the points represent water saturated sediments. Remaining resistivity measurements are converted to formation factor. The data is plotted by porosity vs. formation factor and a best fit line is determined using the least squared error regression method with a constrained at 0.5 to 1. The resulting power equation from this regression yields a as the coefficient and m and the negative of the exponent.

A study showed that the saturation exponent is approximately 2 for various water saturated sediments (Pearson, 1983), but there are studies that support the idea that N can vary significantly in hydrate-bearing sediments. Spangenberg (2001) suggests that it can range from 0.5 to 4 depending on the assumed hydrate cementation method and degree of saturation. For the sites we are processing, we assume N equal to 4, to account for high hydrate saturations.

The water saturation for each point is calculated through the use of Archie's Law. For the first iteration, core-derived chloride concentrations are used to determine fluid resistivity. After a few iterations, the water saturation converges on a final value. The initial salinity is corrected after each iteration through this equation, and the corrected salinity is used in the next iteration:

$$C_{in-situ} = C_o / S_w$$

Where $C_{in-situ}$ is the corrected, in-situ salinity (ppm) and C_o is the initial, core-derived salinity (ppm). This salinity correction is necessary, because the core-derived salinity is not indicative of the in situ salinity. Removing a core from its in situ conditions causes hydrate dissociation. This releases water back into the pore space, significantly decreasing the pore water salinity.

The salinity required for three-phase equilibrium is determined through the combination of classic thermodynamic models by Henry (1999) and Duan (1992). Two of the three stability conditions are assumed to be constant and the third condition is varied until the equilibrium is determined. We assume that the pressure and temperature at a particular depth remain constant regardless of hydrate formation (CITATION). This allows the three-phase equilibrium salinity to be determined throughout the sediment column.

iii. Results

Three sites have been processed using the method described above: a) ODP Site 1249 at Hydrate Ridge, b) ODP Site U1328 at Vancouver Island, and c) NGHP Site 10 in the Krishna-Godavari Basin. The results from these sites are contained in Figures 1, 2, and 3 below. Each figure shows a graph with the Archie-calculated hydrate saturation for the site and a plot of the core-derived salinity, the in situ salinity, and the modeled salinity required for three-phase equilibrium for the site.

All sites exhibit a correlation between increased hydrate saturation and elevated in situ salinity. ODP Site 1249 shows a peak hydrate saturation of approximately 80 percent at 10 mbsf, followed by a large section of high hydrate saturation (40 – 80 percent) between 15 and 50 mbsf. There is a region from 28 to 50 mbsf where salinity values are near to or greater than those necessary for three-phase equilibrium. ODP Site U1328 shows a small section of high hydrate saturation (40 – 80 percent) between 4 and 29 mbsf followed by essentially no hydrate saturation below 50 mbsf. Other than a few peaks, the salinity at this site is significantly lower than those required for three-phase equilibrium. NGHP Site 10 lacks essential data shallower than 23 mbsf, so hydrate saturation could not be calculated for this section. The site shows a large section of high hydrate saturation (20 – 80 percent) between 29 and 158 mbsf (base of GHSZ). The in situ salinities for this zone of high hydrate saturation exceed or are near those required for three-phase equilibrium and follow the trend of the equilibrium salinity line.

iv. Discussion

We hypothesized that elevated in situ salinities from hydrate formation would push the hydrate system towards thermodynamic three-phase equilibrium. From the results presented here, three important trends are evident: a) The strong correlation between hydrate saturation and salinity. b) The decrease in hydrate saturation with depth at ODP Site 1249 and NGHP Site 10. c) The proximity of in situ salinity to those required for three-phase equilibrium at ODP Site 1249 and NGHP Site 10.

All study sites showed a strong correlation between increased hydrate saturation and in situ salinity, supporting the idea of salt exclusion as an explanation for elevated salinities. Arguments have been made that this explanation could be invalid in environments with high rates of groundwater flow, because the elevated salinities would be flushed with seawater as they developed. We believe, however, that the formation of hydrate will significantly reduce the permeability of the host sediment eliminating groundwater flow as a controlling factor (Daigle and Dugan, 2011). If groundwater flow was flushing out these systems, all three conditions for hydrate stability would remain constant and hydrate would saturate fully. This correlation between hydrate saturation and salinity, along with the fact that none of these systems are fully saturated, illustrates the volumetric

relationship between salinity and saturation that would only occur if salt was being excluded and remaining in the pore space.

ODP Site 1249 and NGHP Site 10 have zones of high hydrate saturation that occupy a large percentage of the GHSZ (~50 percent and 95 percent, respectively). In both cases, the hydrate saturation and salinity decrease with depth. This trend supports the “bottom-up” hydrate formation model described in other theoretical studies (Daigle and Dugan, 2010; Liu and Flemings, 2006):

- Initially, no hydrate has formed.
- Gas begins to enter the GHSZ from deeper sediments and is incorporated into the hydrate structure.
- In situ salinity begins to increase near the base of the GHSZ.
- Elevated salinities push the system to the three-phase boundary.
- No more hydrate can form so gas flows through the system, deeper into the GHSZ where more hydrate can form.

This process repeats until the entire GHSZ is saturated to the three-phase boundary. In this model, the hydrate saturation is controlled by the salinity required for three-phase equilibrium. According to the thermodynamic model for these types of systems, the equilibrium salinity values will decrease with depth, resulting in hydrate saturation profiles that also decrease with depth (Liu and Flemings, 2006).

ODP Site 1249 and NGHP Site 10 have in situ salinity values that exceed or are near to the three-phase boundary for a large depth range within the GHSZ. ODP Site U1328 exhibits in situ salinities that are significantly lower than those required for three-phase equilibrium. The proximity of the in situ salinities to this boundary provides important information on the current and potential thermodynamic state of the system. Sites that have salinities close to the three-phase boundary can be assumed to be at three-phase equilibrium. Sites at or near equilibrium are more sensitive to fluctuations of in situ conditions that could push the base of the GHSZ up and cause dissociation. This understanding is important for predictions in climate change models, geohazards, and gas hydrate production technology.

v. Closing Points

We strive to gain understanding into the current state of many hydrate systems around the world and to create a comprehensive and public database for our results. Development of a method to accurately calculate the in situ hydrate saturation and salinity in a variety of environments is imperative for this task. We have presented the current state of the method, the results from three sites, and the implications and understanding gained from those sites. The two issues and possible solutions we see with this method, as it currently stands, are:

- Using a saturation exponent of 4 has some scientific support (Spangenberg, 2001), but is still a relatively broad assumption considering the range of environments and hydrate saturations that are found in nature. To correct this, we are developing a quantitative method for determining saturation exponent.
- Archie’s Law is based upon clean, water-saturated sands. None of the sites we are looking at fit this description. The presence of clay and silt particles has a significant effect on both the

resistivity and porosity of the formation. We are using this method to determine water saturation because is highly supported in literature, despite this limitation. In the coming months, however, we will be looking into using Simandoux's Equation to determine water saturation while accounting for the shale volume in the formation (Simandoux, 1963). We are also considering developing an alternative method of determine hydrate saturation using acoustic log data.

This method has produced reasonable and interesting results that have provided good insights into the state of natural systems. In the future, we expect only greater understanding of hydrate formation in a continuously more diverse set of natural systems.

B) Quantification of saturation exponent in hydrate-bearing sediments

i. Introduction

We are developing an approach to better quantify the saturation exponent, used in Archie's Law, within hydrate-saturated sediments, so that water saturation can be more accurately predicted from log data. There is relatively little information, however, regarding the critical controls on the saturation exponent:

Hydrate Saturation Effect: A study by Spangenberg (2001) modeled the effect of various grain packs and cementation models on the saturation exponent of the sediment. The results suggested that, independent of the cementation model, grain size distribution, or porosity, saturation exponent will tend to increase with increasing hydrate saturation. The magnitude of this effect is primarily controlled by the mechanism of hydrate precipitation in the pore space.

Cementation Model Effect: Two models commonly proposed are isopachous and nodular cementation (Figure 4). The first model suggests that the hydrate would coat the grain surface with the residual pore fluid isolated to the remaining pore space. The nodular cement model suggests that hydrate nucleates within the pores and slowly grows outwards, occupying increasing amounts of pore volume, while the pore fluid acts as the wetting phase in a continuously thinning layer on each grain. One study, by Ecker, et al. (1998), used seismic AVO to estimate rock physics properties of hydrate-bearing sediments and concluded that the only method of hydrate formation that could explain the observed seismic record was if hydrate formed as nodular cement within the pore space. This result is supported by another study concerned with the acoustic properties of hydrate-bearing sediments that suggests that hydrate may be in contact with the grains, but is distinctly not the wetting phase (Winters, et al., 2004).

We present past studies concerned with quartz isopachous cement and carbonate nodular cement whose data have been modified to gain insight on how hydrate saturation affects the saturation exponent. The different cement types are considered to be analogous to the different cementation methods, allowing for comparison between the resulting trends in saturation exponent and those that are reasonable in field conditions.

ii. Method

Data was digitized from papers that described the relationship between porosity and formation factor in rocks dominated by each cementation model. From these data, the cementation exponent for the material could be estimated from their slope. The data were then translated into water saturation vs. resistivity index (I_R) through the following equations:

$$I_R = F_i / F_0$$

$$1 - S_w = S_s = \sum_{i=2}^{i=n} \frac{\theta_{i-1} - \theta_i}{\theta_0}$$

Where I_R is the resistivity index, F_i is the formation factor of the current iteration, F_0 is the initial formation factor, S_s is the solid matrix saturation, θ_i is the porosity of the current iteration, and θ_0 is the initial porosity. The data were arranged by decreasing porosity and the formation factors were scaled by the initial formation factor. The changes in porosity were used to determine a volumetric ratio of solid matrix to remaining pore space. The saturation exponent for the material could then be estimated by taking the slope of the points.

iii. Isopachous Quartz Cement

Quartz diagenesis in sandstones occurs through the coating of grains with a cementing precipitate of non-conductive quartz. This process forms an isopachous cement around each grain, making it a good analogous material for the formation of hydrate in the fashion. Wong, et al. (1984) took glass beads of different grain size categories, fused them together to create samples of different porosities, ranging from 0.4 to 0.01, and then determined the formation factor for each sample. The pertinent results from this experiment are shown in Figure 5. The data were then processed and divided into sections by water saturation (Figure 6). There are three important things to notice about this figure:

- There is a distinct increase in saturation exponent at lower water saturations.
- As a result of the translation between the original data and the data presented in Figure #, the x-axis values were stretched resulting in an overall decrease in slope.
- For the range of water saturation available (0.1 – 1), the saturation exponent does not reach experimental values show in Spangenberg (2001).

Although the saturation exponent for this analogous material does not reach the values used in Lui and Flemings (2006), the data does support the idea that saturation exponent will increase with decreasing water saturation.

iv. Nodular Carbonate Cement

Carbonate diagenesis in sandstones occurs through the nucleation of the carbonates in the pore space and continual growth of the non-conductive carbonate within the voids, making this a good analogy for hydrate precipitating in this manner. Focke and Munn (1987) classified various diagenetic limestone structures in dolomitic sands and measured their permeability. For each sample, the porosity and formation factor were determined so that the cementation exponent could be estimated. The results from this experiment are shown in Figure 7. These data were then processed and plotted to determine the saturation exponent (Figure 8). The preliminary results show that saturation exponent decreases at lower water saturations. We believe that this could indicate two things: a) that these data do not accurately represent the nodular formation of hydrate, or b) that it is incorrect to assume that saturation exponent will increase with lower water saturations. Further investigation is necessary to clarify which of these ideas is correct.

v. Closing Points

The current state of research on this topic shows some promising, preliminary results that are improving our understanding of how the saturation exponent acts in hydrate-saturated sediments. Future work includes:

- Determine if a relationship exists between cementation coefficient, water saturation, and saturation exponent in isopachous cement that would allow us to estimate saturation exponent from the cementation coefficient.
- Impose the values of saturation exponent we desire and see what types of natural cementation models produce the related cementation coefficients.
- Examine data in high porosity ranges to see how the water saturation/saturation exponent relationship will act in shallower sediments.
- Continue the investigation of carbonate nodular cement as an analogy for a water-wet hydrate formation model.

From the knowledge we have already gained on saturation exponent, we are confident that this research will help develop a better method for determine saturation exponent for these systems.

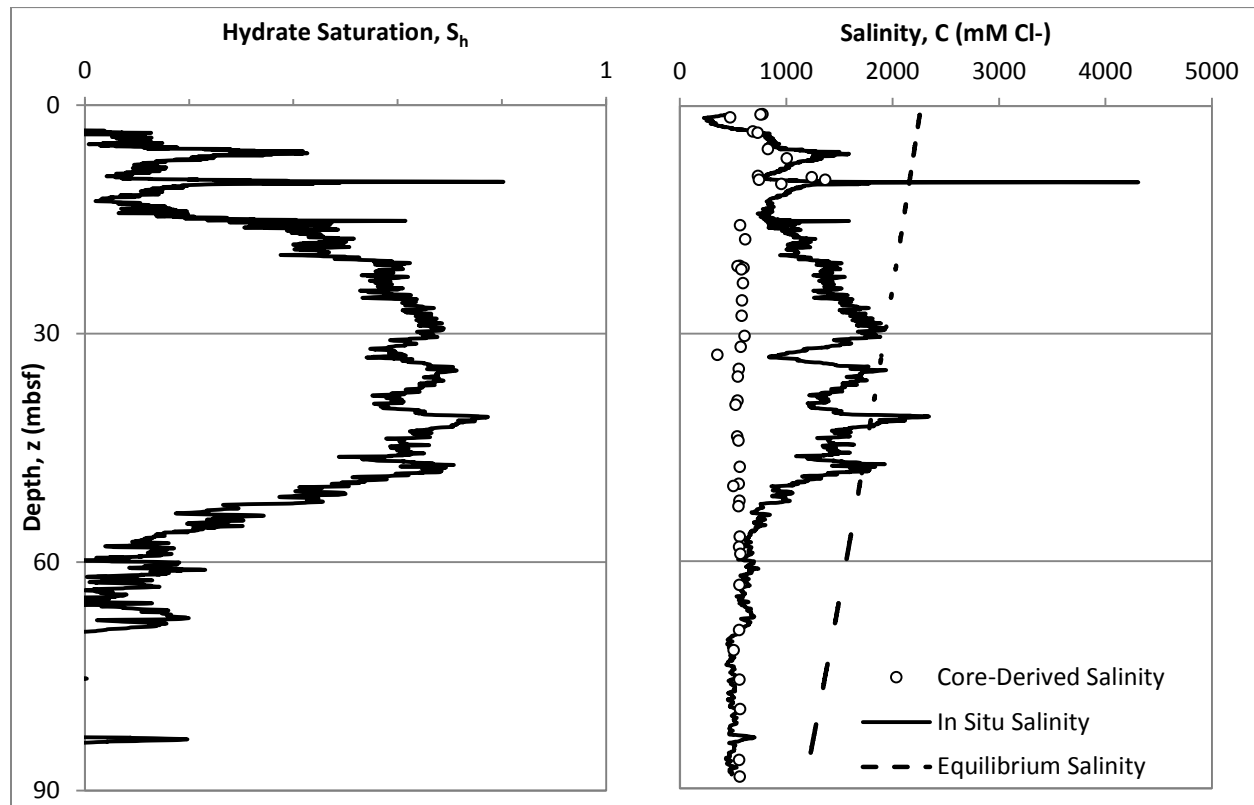


Figure 1: Archie calculated in situ hydrate saturation and salinity for ODP Site 1249.

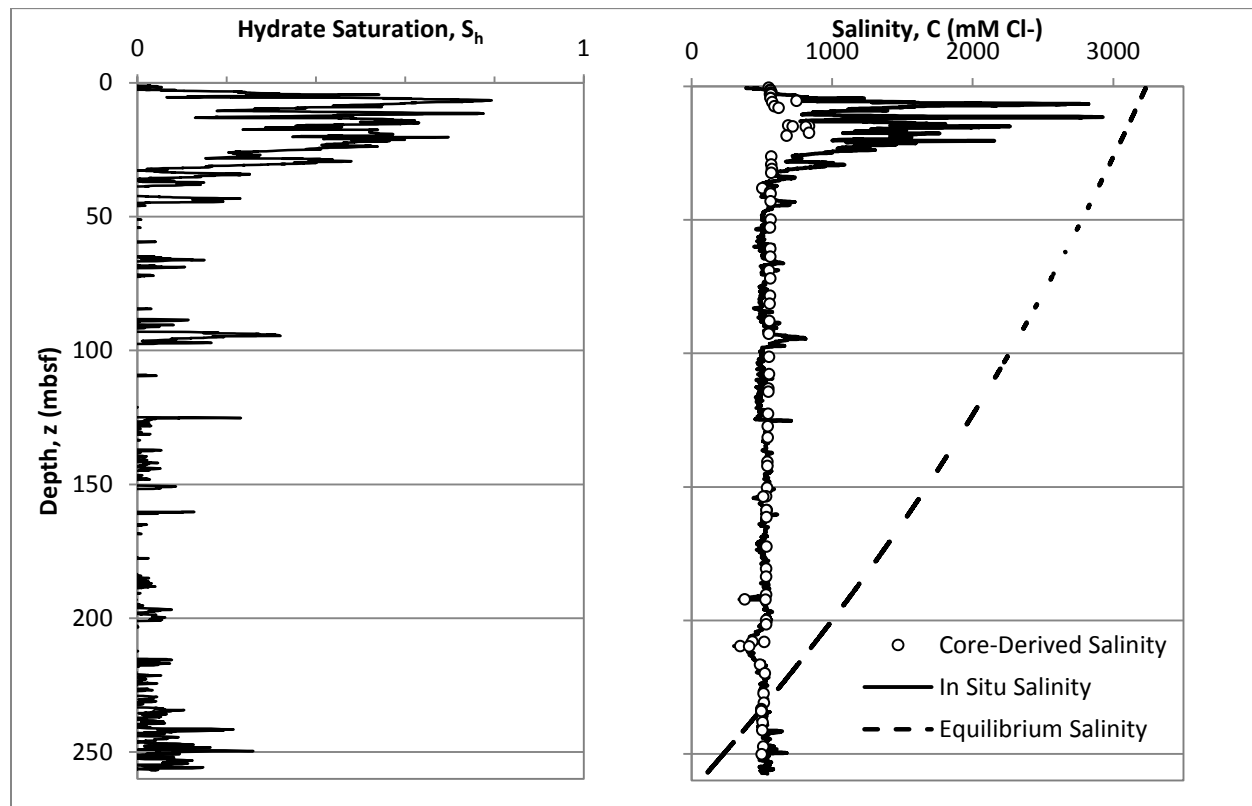


Figure 2: Archie calculated in situ hydrate saturation and salinity for ODP Site U1328.

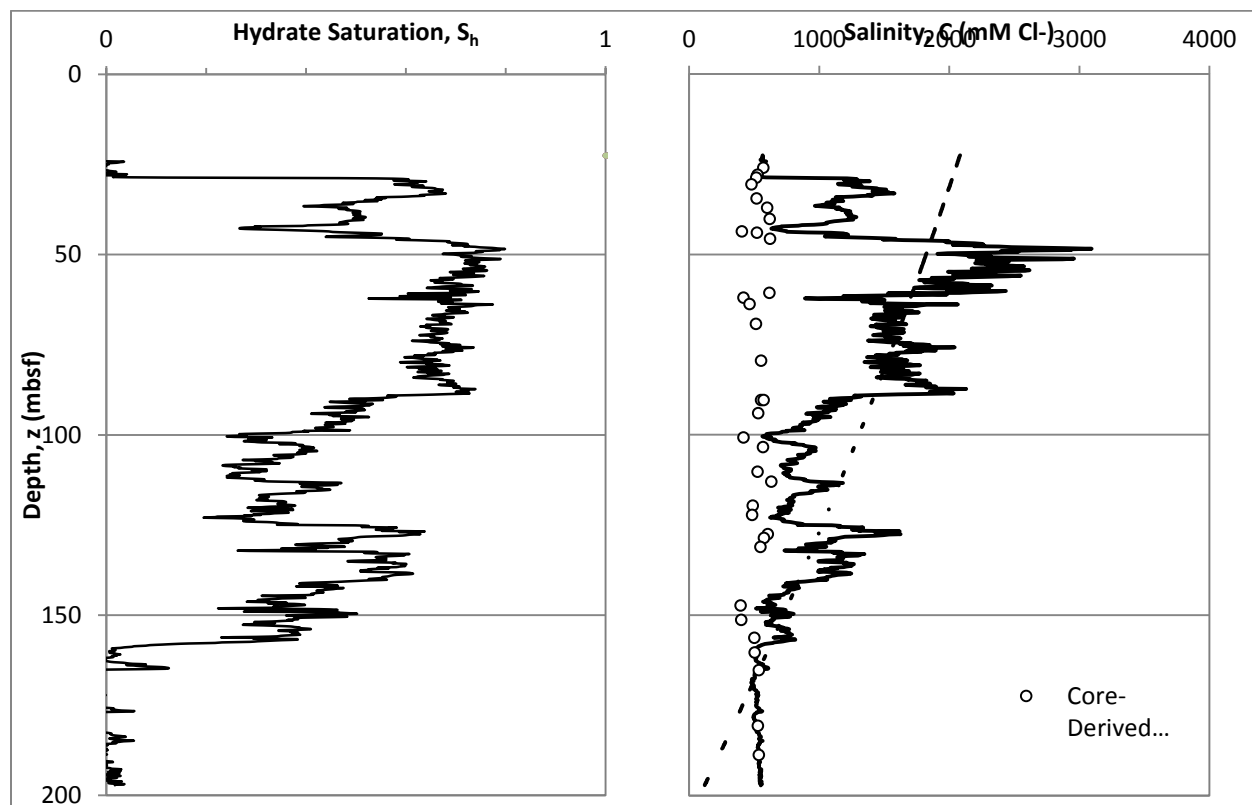


Figure 3: Archie calculated in situ hydrate saturation and salinity for NGHP Site 10.

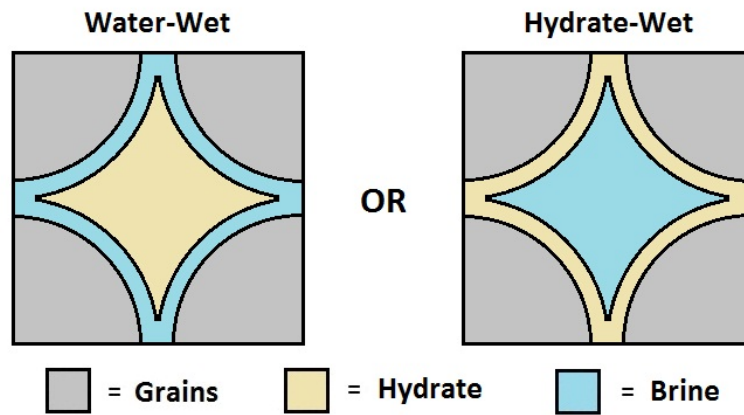


Figure 4: Diagram showing the difference between isopachous (hydrate-wet) and nodular (water-wet) cementation models

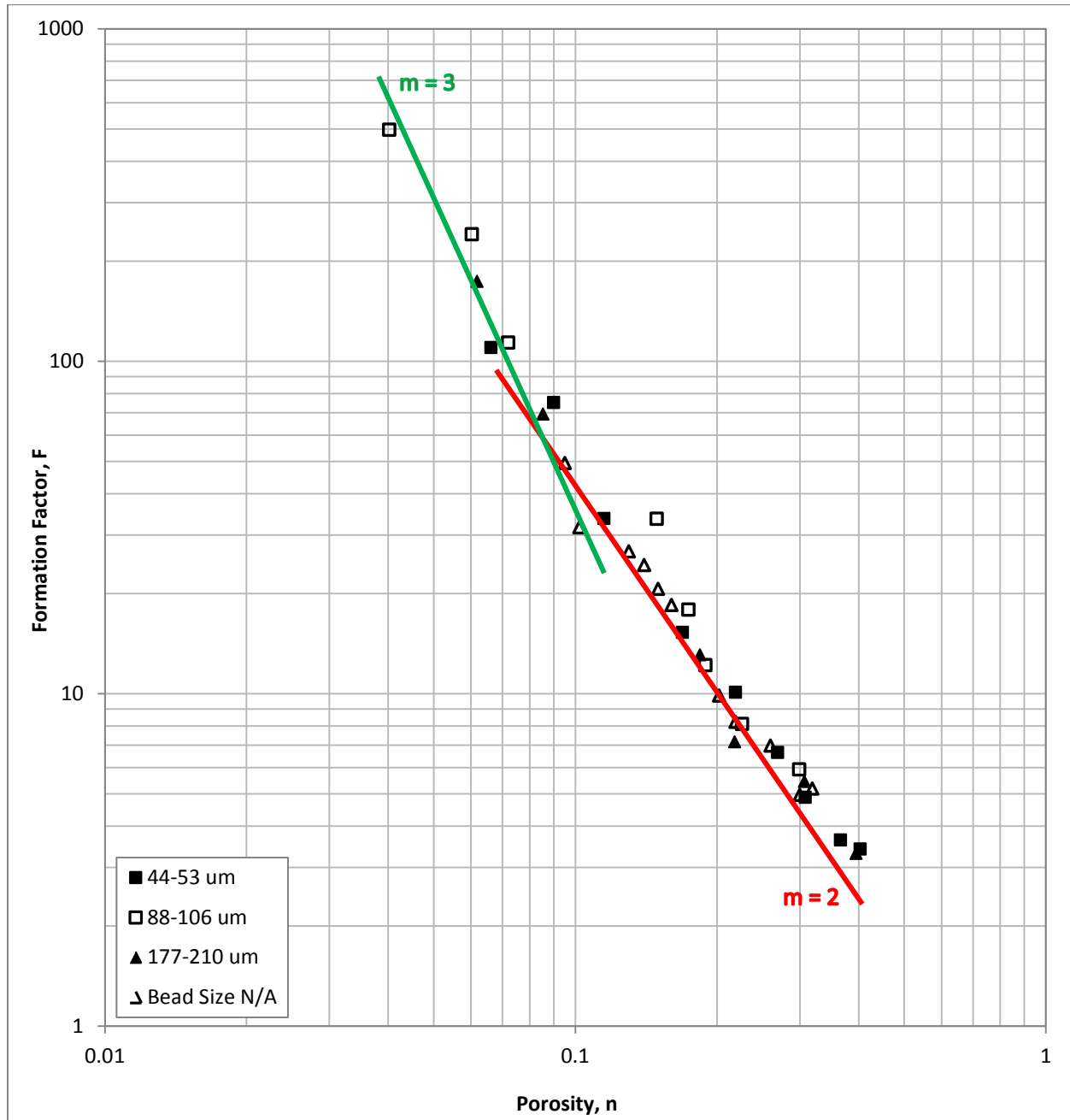


Figure 5: Data digitized from Bryant and Pallatt, 1996 concerning the effect of porosity changes, as a result of isopachous quartz cement formation, on the formation factor. Red and green lines show a slope of 2 and 3, respectively, for cementation exponent estimation.

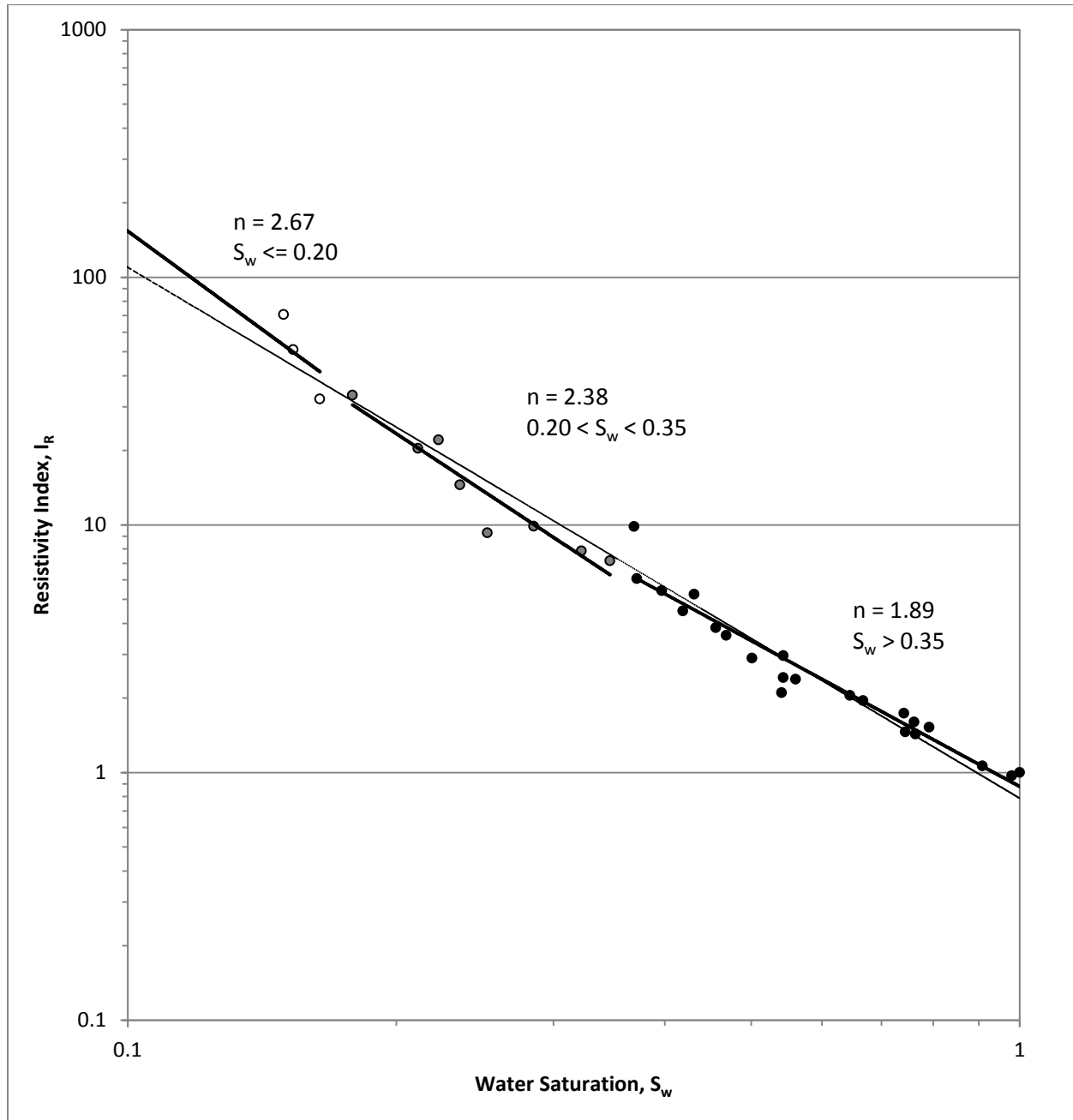


Figure 6: Water saturation and resistivity index data, translated from Bryant and Pallatt, 1996, for isopachous quartz cement. Data is broken up into sections at water saturations 0.35 and 0.2 to show how slope and saturation exponent change with water saturation. Dashed line shows the saturation exponent for all the available data. Solid lines show the saturation exponent for each section of the water saturation filtered data.

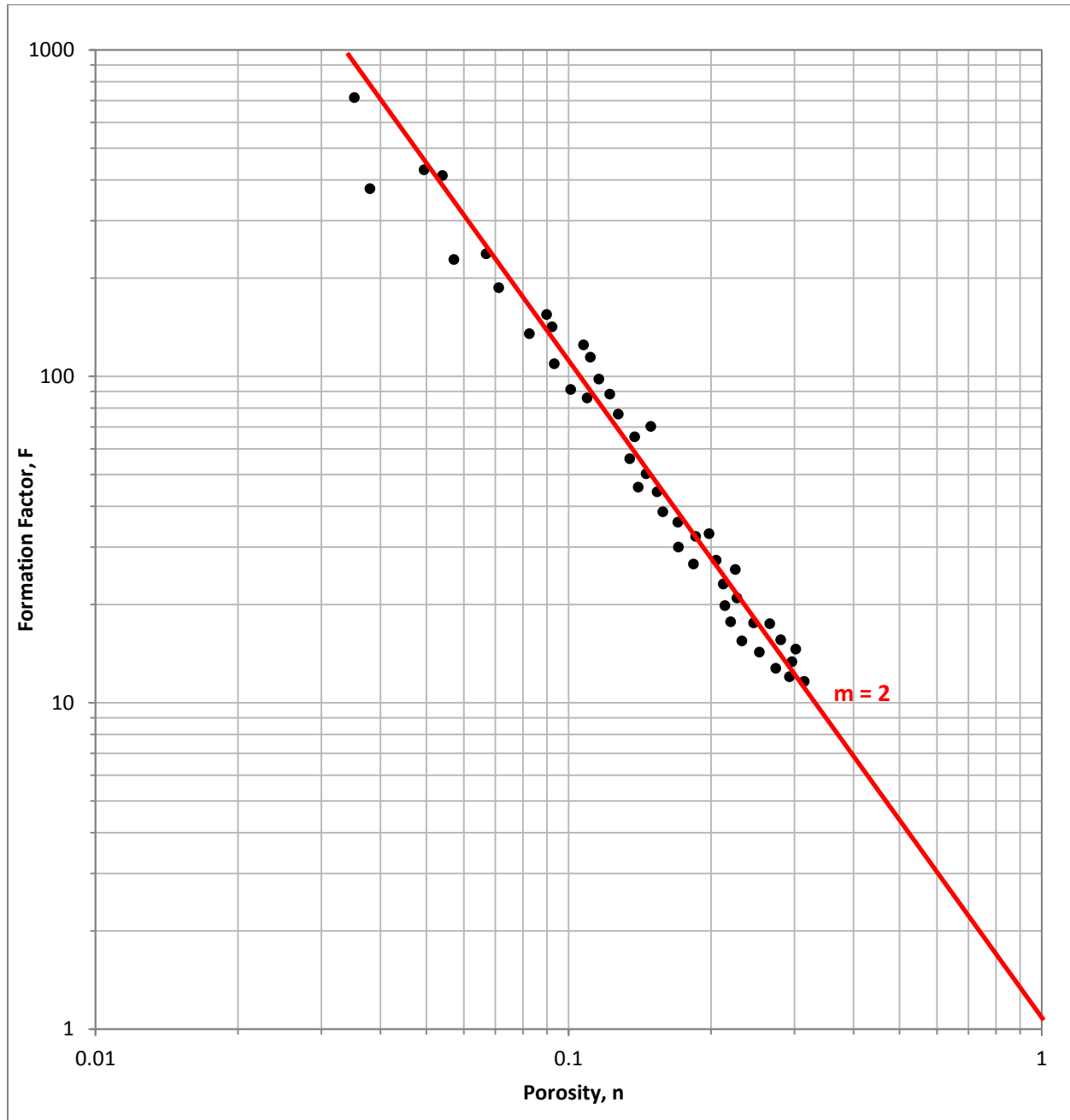


Figure 7: Data digitized from Focke and Munn (1987) concerning the effect of porosity changes, as a result of nodular carbonate cement formation, on the formation factor of intergranular, lime and dolomite grainstones. Red line shows a slope of 2 for cementation exponent estimation.

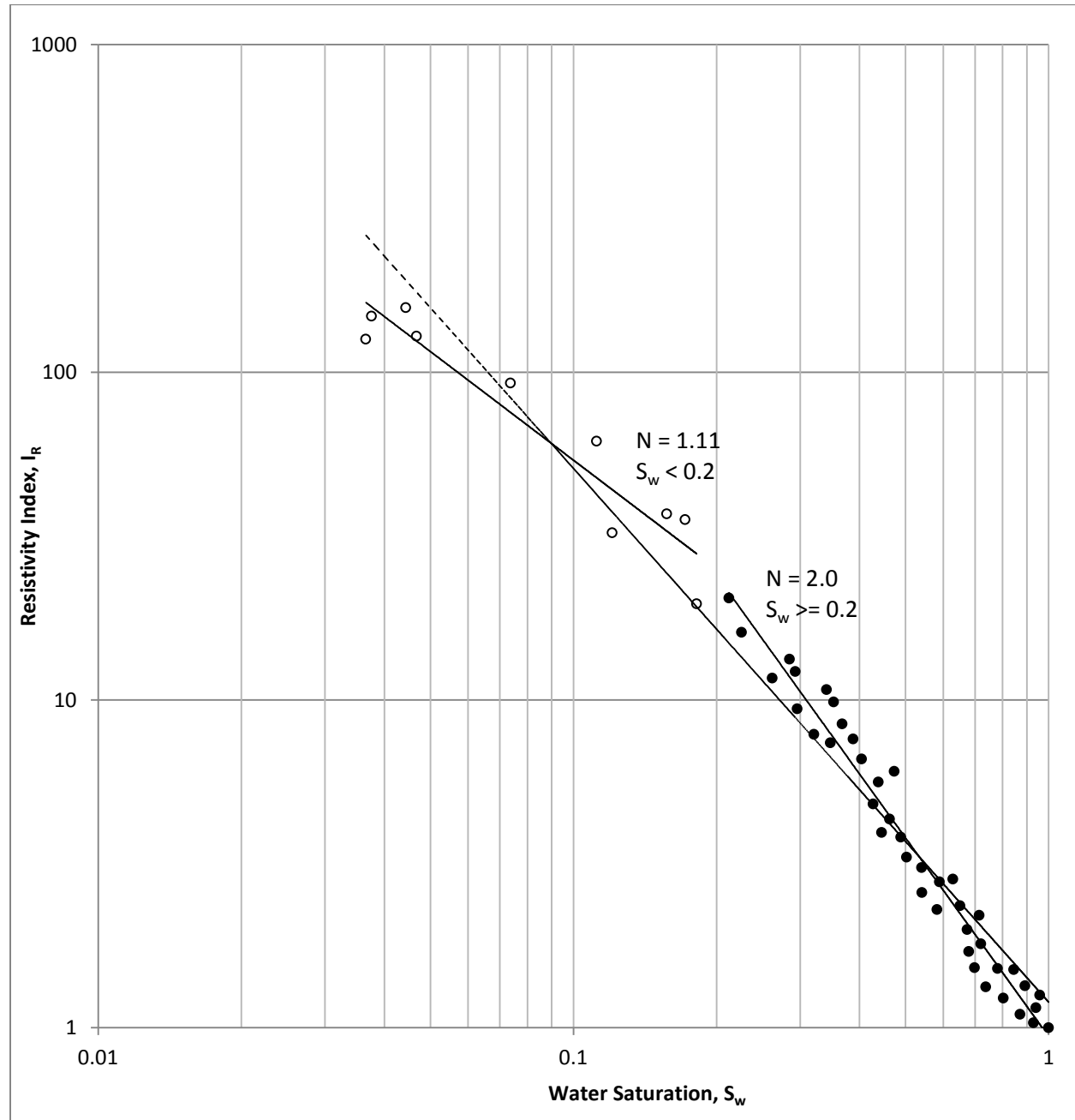


Figure 8: Water saturation and resistivity index data, translated from Focke and Munn (1987), for nodular carbonate cement. Data is broken up into sections at water saturation 0.2 to show how slope and saturation exponent change with water saturation. Dashed line shows the saturation exponent for all the available data. Solid lines show the saturation exponent for each section of the water saturation filtered data.

References:

- Archie, G.E., The Electrical Resistivity Log as an Aid in Determining Some Reservoir Characteristics, Transactions of AIME, 146 (1942), pp. 54 – 62.
- Arps, J.J., 1953, The Effect of Temperature on the Density and Electrical Resistivity of Sodium Chloride Solutions, Journal of Petroleum Technology, 5 (10), pp. 17 – 20.
- Bryant, S. and Pallatt, N., 1996, Predicting formation factor and resistivity index in simple sandstones, Journal of Petroleum Science and Engineering, 16, pp. 196 – 179.

- Collett, T. S., et al., 2012, Gulf of Mexico Gas Hydrate Joint Industry Project Leg II logging-while-drilling data acquisition and analysis, *Marine and Petroleum Geology*, 34, pp. 1 – 3.
- Cook, A., et al., 2010, Electrical anisotropy due to gas hydrate-filled fractures, *Geophysics*, 75 (6), pp. F173 – F185.
- Cook, A., et al., 2012, Electrical anisotropy of gas hydrate-bearing sand reservoirs in the Gulf of Mexico, *Marine and Petroleum Geology*, 34, pp. 72 – 84.
- Daigle, H. and Dugan, B., 2010, Effects of multiphase supply on hydrate accumulation and fracture generation, *Geophysical Research Letters*, 37, 5 pages.
- Daigle, H. and Dugan, B., 2011, Capillary controls on methane hydrate distribution and fracturing in advective systems, *Geochemistry Geophysics Geosystems*, 12 (1), 18 pages.
- Duan, Z., et al., 1992, The prediction of methane solubility on natural waters to high ionic strength from 0 to 250°C and from 0 to 1600 bar. *Geochimica et Cosmochimica Acta*, 56, pp. 1451 – 1460.
- Ecker, C., Dvorkin, J., and Nur, A., 1998. Sediments with gas hydrates: Internal structure from seismic AVO, *Geophysics*, 63(5), pp. 1659 – 1669.
- Focke, J. W. and Munn, D., 1987. Cementation exponent in Middle Eastern carbonate reservoirs
- Henry, P., 1999, Formation of natural gas hydrates in marine sediments 2. Thermodynamic calculations of stability conditions in porous sediments, *Journal of Geophysical Research*, 104 (B10), pp. 23005 – 23022.
- Liu, X. and Flemings, P. B., 2006, Passing gas through the hydrate stability zone at southern Hydrate Ridge, offshore Oregon, *Earth and Planetary Science Letters*, 241, pp. 211 – 226.
- Pearson, C. F., et al., 1983, Natural Gas Hydrate Deposits: A Review of In Situ Properties, *Journal of Physical Chemistry*, 87, pp. 4180 – 4185.
- Simandoux, P., 1963, Dielectric measurements in porous media and application to shaly formation, *Revue de L'Institut Français du Pétrole*, 18, Supplementary Issue, pp. 193 – 215.
- Spangenberg, E., 2001, Modeling of the influence of gas hydrate content on the electrical properties of porous sediments, *Journal of Geophysical Research*, 106 (B4), pp. 6535 – 6548.
- Winters, W. J., et al., 2004, Physical properties and rock physics models of sediment containing natural and laboratory-formed methane gas hydrate, 89, pp. 1221 – 1227.

Task 4: Laboratory Evaluation of Hydrate Dissociation:

- Subtask 4.1 - Freezing to 3 phase stability conditions, followed by melting from above
- Subtask 4.2 - Freezing to L+H condition, warming from above
- Subtask 4.3 - Freezing to L+H condition, warming from below

We have constructed two thermistor strings. The thermistor string consists of ten thermistors mounted every 10 cm on a rod, which is epoxied inside of a 0.25" OD tube. The thermistor wires are passed through a strain relieving circular connector and wired into a National Instruments 16-bit DAQ. Each thermistor is powered by a 5 VDC outlet on the DAQ. This allows is to monitor temperature on all ten thermistors at the same time, using a single device. To date, the thermistor strings have been tested in warm, cold, and near-freezing conditions with good agreement between each thermistor.

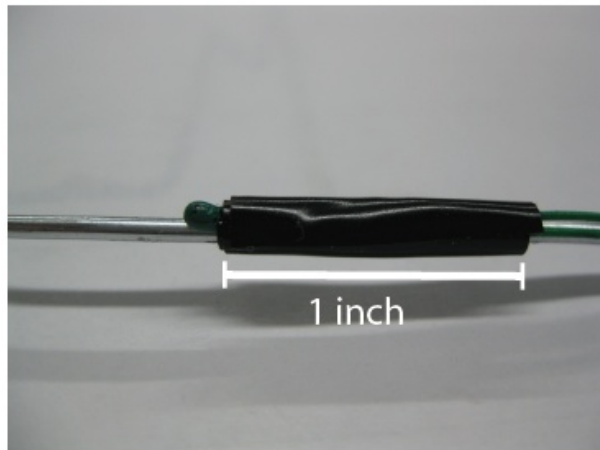


Figure 9: Individual 10 K Ω thermistor mounted on inner rod of thermistor string.

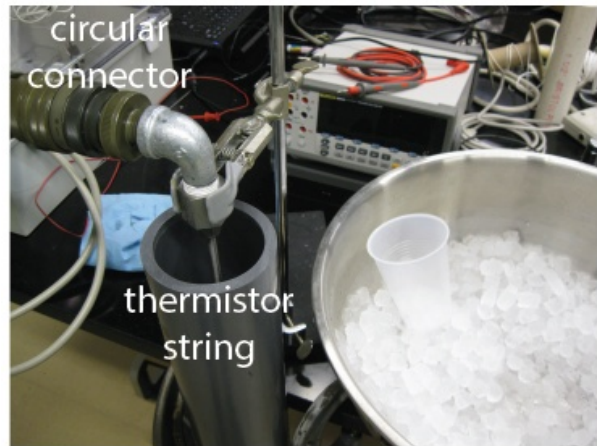


Figure 10: Thermistor string suspended inside pipe prior to ice bath calibration.

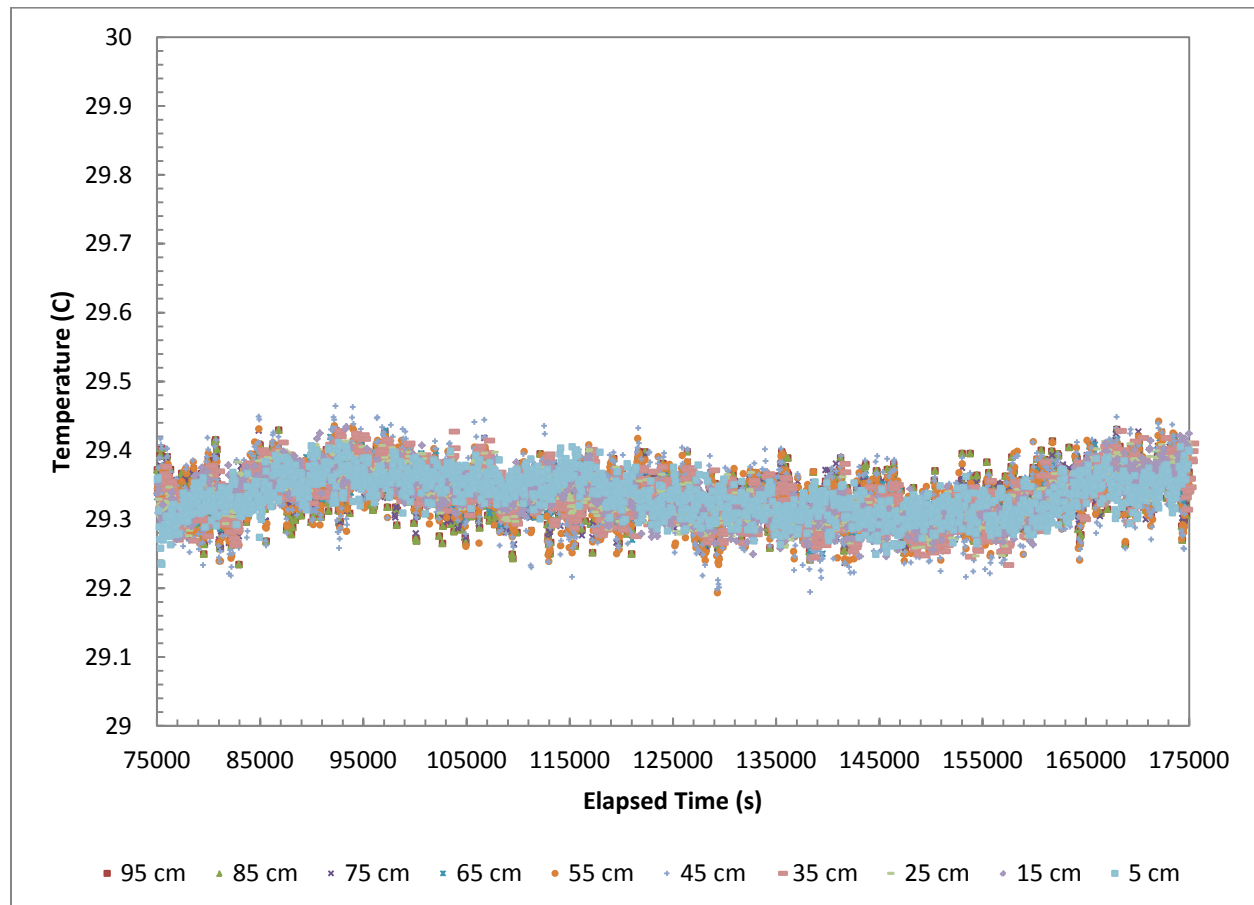


Figure 11: Example of data collected by one of the thermistor strings. The length in centimeters (95 cm, 85 cm, etc.) refers to the location in the thermistor string. The thermistor at 5 cm is closest to the circular connector (base of string), the 95 cm thermistor is near the tip.

What opportunities for training and professional development has the project provided?

There have been several conversations between several researchers working on this grant, including a site visit by a UT research scientist associate and LBNL research scientist. Through these one-on-one interactions, the LBNL scientist was able to share their knowledge and experience related to CT scanning and image analyses, as well as the process of running hydrate formation experiments with the UT research scientist associate. A graduate student has been trained in interpretation of log and core data to determine hydrate saturation.

How have the results been disseminated to communities of interest?

An abstract titled, *In situ gas hydrate saturation and salinity of hydrate-bearing sediments through well log analysis*, has been submitted to the Society of Petrophysicists and Well Log Analysts (SPWLA) conference during June 2013.

What do you plan to do during the next reporting period to accomplish the goals?

Task 1: Project Management and Planning:

Experiment plan:

Test Setup 7/9/2013 – 7/19/2013

Test setup includes temperature measurement string development (nearly complete at UT), resistivity string development (under way at LBNL), vessel preparation including corrosion protection and modification of temperature control system (initiated at LBNL).

Test Subtask 4.1 7/22/2013 - 8/16/2013

Subtask 4.1 - Freezing to 3 phase stability conditions, followed by melting from above

The experimental vessel will be filled with coarse sand, or with alternating layers of coarse and very fine sand to provide capillarity and permeability contrast, and then X-ray CT scan the vessel. The vessel will then be saturated with simulated seawater and re-scanned. Temperature control for gas-brine stability (no hydrate) shall be established. Gas shall be introduced into the top of the vessel through a mass flow controller. Seawater shall be slowly withdrawn out the bottom using a high-pressure syringe pump. A scan of P-wave velocity along the column, combined with an overall mass balance on each phase permits estimating the initial saturation profile in the column. The temperature control, through a set of individual cooling jackets distributed along the outside of the column shall then be activated so that successive sections of the column become “cool”, starting from the top section. In this fashion the base of gas hydrate stability is caused to move at a prescribed rate (about 10 to 100 cm/day) down the column. Hydrate formation will increase salinity such that three-phase equilibrium occurs throughout the column, with the “cool” temperature selected to insure that concentrated (approximately 2x) brine remains. Temperatures, pressures, and resistances shall be recorded frequently (~ every 30 sec) and ultrasonic (P wave) velocities shall be collected by hand regularly (~daily). The column shall remain connected to an external reservoir of brine and gas that allows gas to leave the column (in response to pressure elevation) and brine to enter the column (to replace fluid phase volumes consumed by hydrate). The mass of fluid in the external reservoir shall be recorded continuously. This data combined with pressure and temperature measurement enable quantification of all fluid movement into/out of the column. The resistances shall be interpreted for the salinity distribution; the P wave velocities shall be interpreted to help understand three-phase saturations; the temperature and pressure shall be interpreted for the locus of three-phase equilibrium in the column and for fluid phase transport. The variation in salinity distribution over time in all the cooled sections shall be closely monitored to assess whether diffusive transport is significant.

Once the entire column is equilibrated at the three-phase stability condition, the vessel shall be rescanned using CT. The temperature control shall then be programmed to raise the temperature at the top of the column slightly above the three-phase stability threshold. When dissociation is underway, as indicated by pressure and temperature changes, the temperature shall be increased in the next uppermost section of the sand column. This process shall be repeated until dissociation is complete. Gas mass flow, temperatures, pressures and P-wave velocities shall be recorded over the dissociation and analyzed to infer hydrate location and phase saturations.

Test Subtask 4.2 Tentatively 8/26/2013 – 9/20/2013

Subtask 4.2 - Freezing to L+H condition, warming from above

An experiment analogous to that in Task 4.1 will be performed to examine the case where gas hydrate is more stable above the base of the gas hydrate stability zone (BGHSZ), with additional cooling applied in the central region of the vessel to increase stability there. Warming from above (akin to a downward moving thermal pulse), shall be performed and results compared with the results from subtask 4.1.

Test Subtask 4.3 Tentatively 9/30/2013 – 10/28/2013

Subtask 4.3 - Freezing to L+H condition, warming from below

Similar to Subtask 4.2, hydrate will be formed to the liquid-brine region (L+H) in the central region. Dissociation shall be induced by warming from below simulating dissociation at the BGHSZ from a slowly downward moving or wide thermal pulse. Results from this task shall be compared to results from Subtasks 4.1 and 4.2.

Task 2: Conceptual and Numerical Model Development -1D:

Subtask 2.1 - Dissociation of 1D vertical hydrate accumulation

Subtask 2.2 - Apply 1D model to laboratory experiment

Subtask 2.3 - 1D models of natural examples

Subtask 2.3.1 Hydrate accumulations below permafrost

Subtask 2.3.2 - 1D model application to deposits near up-dip limit of stability zone on continental margins

Continue model development.

We have received the numerical code of the dynamic multiphase flow model of hydrate formation. We plan to adapt this code to capture the specific dynamical situation that will occur in the experimental apparatus.

Task 3: Categorize stability of known hydrate reservoirs:

Over the next three months we will be advancing our knowledge of this topic on three fronts. Firstly, we will continue to collect and process data from hydrate systems around the world to expand our database of defined hydrate systems. Our area of focus includes, but is not limited to: 10 additional sites drilled during the Indian National Gas Hydrates Project (NGHP), 4 sites drilled during the Ulleung Basin Gas Hydrates Project II (UBGH2), the Mallik 5L-38 gas hydrate production well, and other ODP sites where hydrates have been recovered. Secondly, we will continue to improve the method used to process these sites and determine the thermodynamic state at each other them. Possible improvements include: Implementing the Simandoux Equation to take into account the volume of shale present in the formation, investigating the use of acoustic logs to determine hydrate saturations, and improving the estimations of Archie's parameters. Any changes to the method will be applied to all past and future sites. Finally, related to the previous improvement, we will continue our research into the quantification of the saturation exponent through the use of other, natural cements as analogies. The saturation

exponent has a significant effect on the calculated hydrate saturation. It is important enough that assuming it to be any particular number for hydrate-saturated sediments is too simplistic. The ability to confidently define saturation exponent will significantly improve the accuracy of our results in this area.

Task 4: Laboratory Evaluation of Hydrate Dissociation:

Subtask 4.1 - Freezing to 3 phase stability conditions, followed by melting from above

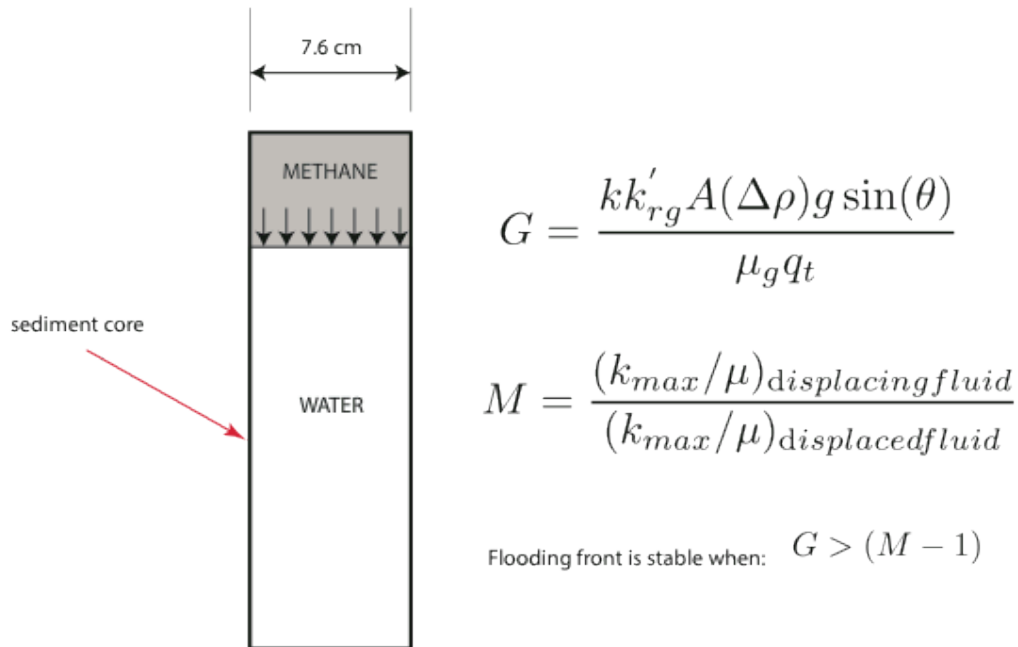
Subtask 4.2 - Freezing to L+H condition, warming from above

Subtask 4.3 - Freezing to L+H condition, warming from below

We will complete the manufacturing of the thermistor and resistivity strings and data acquisition system. We will run these systems through a series of diagnostic tests, calibration exercises, and deliver them to LBNL for use in the laboratory portion of this project.

Upon completion of pressure tests, the thermistor strings and DAQ system will be shipped to Dr. Kneafsey at Lawrence-Berkeley National Laboratory (LBNL) where they will be incorporated into an already existing temperature controlled high pressure chamber. These strings, in addition to a companion resistivity string being developed at LBNL will be used to monitor temperature and resistivity inside of the chamber as the hydrate stability zone migrates through a brine saturated sediment column.

The preliminary step for experiments of core-scale hydrate production is to produce a gas-saturated sediment core. This gas-saturated core is produced by first water-saturating the sediment core and then injecting gas at a steady rate to produce a stable, continuous gas front that floods the core. We plan to perform this gas saturation in a circular core composed of F110 Sand with permeability 8.4×10^{-13} and with cross-sectional area, 45 cm^2 . The flooding will be performed from the top of a vertically oriented core. We consider this gas flooding as an immiscible displacement of water by gas and make use of the Buckley-Leverett equations. Under the Buckley-Leverett equations, it is assumed that a steady shock front separating the two phases propagates through the core. This front is susceptible to viscous fingering at high injection rates. The injection rate can be reduced to prevent this viscous fingering and to provide a continuous stable front. The critical injection rate is set by the Buckley-Leverett analysis and describes the competition between the viscous mobility of the phases and the stabilizing effects of gravity. For the geometries and physical properties described, we can ensure stability with injection rates below $\sim 1.45 \text{ mL/min}$.



where

- k absolute permeability
 k'_{rx} maximum relative permeability of phase x
 A cross-sectional area
 $\Delta\rho$ density difference between phases
 θ angle of inclination
 μ_x kinematic viscosity of phase x
 q_t injection rate

PRODUCTS:

What has the project produced?

Nothing to report

PARTICIPANTS & OTHER COLLABORATING ORGANIZATIONS:

What individuals have worked on the project?

Provide the following information for: (1) principal investigator(s)/project director(s) (PIs/PDs); and (2) each person who has worked at least one person month per year on the project during the reporting period, regardless of the source of compensation (a person month equals approximately 160 hours of effort).

Name	Peter Flemings	Steve Bryant	Tim Kneafsey	Dylan Meyer	Donnie Brooks
Project Role	Principal Investigator	Co-Principal Investigator	Co-Principal Investigator	Graduate Student	Laboratory Assistant

Nearest person month worked	.25	.25	.25	1	1
Contribution	Advised graduate student Meyer, managed project, and recruited students. Worked with technicians for thermistor development.	Advised graduate student Meyer on analysis of models of pore space alteration due to hydrate growth and its effect on saturation exponent.	Participated in conference calls on experimental design.	Performed analysis of thermodynamic state of 3 locations.	Built a prototype thermistor string.
Funding Support	The University of Texas	The University of Texas	Lawrence Berkeley National Lab	UTIG Fellowship	The University of Texas
Collaborated with individual in foreign country	No	No	No	No	No

What other organizations have been involved as partners?

Organization Name: Lawrence Berkeley National Lab

Location of Organization: Berkeley, CA

Partner's contribution to the project (identify one or more)

- In-kind support (e.g., partner makes software, computers, equipment, etc., available to project staff);
- Facilities (e.g., project staff use the partner's facilities for project activities);
- Collaborative research (e.g., partner's staff work with project staff on the project); and

Have other collaborators or contacts been involved?

No

IMPACT:***What is the impact on the development of the principal discipline(s) of the project?***

Geological models of gas transport and hydrate melting and solidification have suggested that free gas cannot migrate through the hydrate stability zone during melting. In contrast, we suggest that free gas can migrate through the hydrate stability zone by altering the conditions of hydrate stability to a state of three-phase equilibrium through the elevation of salinity and possibly temperature. This results in fundamentally different macro-scale behavior during melting and may result in greater gas venting than has been previously demonstrated. If this hypothesis is correct, it may engender a new generation of field and laboratory investigations to document this behavior in both the field of geosciences and petroleum engineering. Second, the project links theoretical development with laboratory modeling because the concepts can be applied at the laboratory scale as well as the field scale. The laboratory experiments to be conducted will enable validation of the mechanisms incorporated in the models. These laboratory experiments will play a key role in demonstrating the processes.

What is the impact on other disciplines?

A likely outcome of our work is a more quantitative prediction of the magnitude of methane flux from the earth to the atmosphere over human (decadal) timescales and geological timescales (10,000 years). These will serve as boundary conditions for atmospheric climate models. In turn, these results may guide policy decisions.

What is the impact on the development of human resources?

We are working at the interface of geosciences and engineering. We are coupling theory and laboratory experiments to address macro-scale geologic problems. This is training a new generation of geoscientists and engineers to think with a systems-based approach that links observation with theory.

The results are being applied in the classroom and the support is training several graduate students.

What is the impact on physical, institutional, and information resources that form infrastructure?

The project is strengthening the experimental efforts and capability at UT as it is our drop to develop sensor equipment. The project is strengthening development at LBNL where primary experimental work is occurring.

What is the impact on technology transfer?

We are presenting our research to approximately 100 industry members at our GeoFluids consortium and we will be presenting at a range of national and international meetings.

What is the impact on society beyond science and technology?

A likely outcome of our work is a more quantitative prediction of the magnitude of methane flux from the earth to the atmosphere over human (decadal) timescales and geological timescales (10,000 years). These will serve as boundary conditions for atmospheric climate models. In turn, these results may guide policy decisions.

What dollar amount of the award's budget is being spent in foreign country(ies)?

Zero percent of the award's budget is being spent in foreign countries.

CHANGES/PROBLEMS:

Changes in approach and reasons for change

No changes in approach to report for this reporting period.

Actual or anticipated problems or delays and actions or plans to resolve them

No problems or delays to report for this reporting period.

Changes that have a significant impact on expenditures

No changes in approach to report for this reporting period.

Significant changes in use or care of human subjects, vertebrate animals, and/or Biohazards

Nothing to report

Change of primary performance site location from that originally proposed

Nothing to report

DOE Award No.: DE-FE0010406

Quarterly Research Performance Progress Report (Period ending 3/31/2012)

CONTROLS ON METHANE EXPULSION DURING MELTING OF NATURAL GAS HYDRATE SYSTEMS: TOPIC AREA 2

BUDGETARY INFORMATION:

	Budget Period 1					
	Q1		Q2		Q3	
	10/1/12 - 2/15/13		2/16/13-6/30/2013		7/1/2013-11/15/2013	
	Q1	Cumulative Total	Q2	Cumulative Total	Q3	Cumulative Total
Baseline Cost Plan						
Federal Share	\$ 136,111.50	\$ 136,111.50	\$ 175,000.50	\$ 311,112.00	\$ 175,000.50	\$ 486,112.50
Non-Federal Share	\$ 43,568.75	\$ 43,568.75	\$ 43,568.75	\$ 87,137.50	\$ 43,568.75	\$ 130,706.25
Total Planned	\$ 179,680.25	\$ 179,680.25	\$ 218,569.25	\$ 398,249.50	\$ 218,569.25	\$ 616,818.75
Actual Incurred Cost						
Federal Share	\$ 45,506.00	\$ 45,506.00	\$ 4,708.00	\$ 50,214.00	\$ -	\$ 50,214.00
Non-Federal Share	\$ -	\$ -	\$ 8,600.00	\$ 8,600.00	\$ -	\$ 8,600.00
Total Incurred Cost	\$ 45,506.00	\$ 45,506.00	\$ 13,308.00	\$ 58,814.00	\$ -	\$ 58,814.00
Variance						
Federal Share	\$ (90,605.50)	\$ (90,605.50)	\$ (170,292.50)	\$ (260,898.00)	\$ (175,000.50)	\$ (435,898.50)
Non-Federal Share	\$ (43,568.75)	\$ (43,568.75)	\$ (34,968.75)	\$ (78,537.50)	\$ (43,568.75)	\$ (122,106.25)
Total Variances	\$ (134,174.25)	\$ (134,174.25)	\$ (205,261.25)	\$ (339,435.50)	\$ (218,569.25)	\$ (558,004.75)
	Budget Period 2					
	Q1		Q2		Q3	
	4/1/2014-8/15/2014		8/16/2014-12/31/2014		1/1/2015-5/15/2015	
	Q1	Cumulative Total	Q2	Cumulative Total	Q3	Cumulative Total
Baseline Cost Plan						
Federal Share	\$ 127,422.00	\$ 661,113.00	\$ 127,422.00	\$ 788,535.00	\$ 127,422.00	\$ 915,957.00
Non-Federal Share	\$ 34,048.50	\$ 174,275.00	\$ 34,048.50	\$ 208,323.50	\$ 34,048.50	\$ 242,372.00
Total Planned	\$ 161,470.50	\$ 835,388.00	\$ 161,470.50	\$ 996,858.50	\$ 161,470.50	\$ 1,158,329.00
Actual Incurred Cost						
Federal Share	\$ -	\$ 50,214.00	\$ -	\$ 50,214.00	\$ -	\$ 50,214.00
Non-Federal Share	\$ -	\$ 8,600.00	\$ -	\$ 8,600.00	\$ -	\$ 8,600.00
Total Incurred Cost	\$ -	\$ 58,814.00	\$ -	\$ 58,814.00	\$ -	\$ 58,814.00
Variance						
Federal Share	\$ (127,422.00)	\$ (610,899.00)	\$ (127,422.00)	\$ (738,321.00)	\$ (127,422.00)	\$ (865,743.00)
Non-Federal Share	\$ (34,048.50)	\$ (165,675.00)	\$ (34,048.50)	\$ (199,723.50)	\$ (34,048.50)	\$ (233,772.00)
Total Variances	\$ (161,470.50)	\$ (776,574.00)	\$ (161,470.50)	\$ (938,044.50)	\$ (161,470.50)	\$ (1,099,515.00)

National Energy Technology Laboratory

626 Cochrans Mill Road
P.O. Box 10940
Pittsburgh, PA 15236-0940

3610 Collins Ferry Road
P.O. Box 880
Morgantown, WV 26507-0880

13131 Dairy Ashford Road, Suite 225
Sugar Land, TX 77478

1450 Queen Avenue SW
Albany, OR 97321-2198

Arctic Energy Office
420 L Street, Suite 305
Anchorage, AK 99501

Visit the NETL website at:
www.netl.doe.gov

Customer Service Line:
1-800-553-7681

